

Diglyme as a Promoter for the Electrochemical Formation of Quaternary Graphite Intercalation Compounds Containing two Different Types of Solvents

Youhyun Son,^[a] Gustav Åvall,^[a, b] Guillermo A. Ferrero,^[a] Annica I. Freytag,^[b] Ines Escher,^[a] Knut Arne Janßen,^[a] Maria Jauregui,^[c, d] Damien Saurel,^[c] Montserrat Galceran,^[c] and Philipp Adelhelm^{*[a, b]}

Co-intercalation using ether-based electrolytes renders graphite as a promising anode material in sodium-ion batteries (SIBs). While most research on electrochemical solvent co-intercalation in graphite has focused on linear ethers such as mono-, di-, tri-, tetra-, and penta-glyme, we herein investigate the possibility of reversible electrochemical co-intercalation with alternative solvents, especially cyclic ethers tetrahydrofuran (THF) and 1,3-dioxolane (DOL), which show no signs of co-intercalation on their own. We demonstrate, however, that this reaction becomes feasible when incorporating diethylene glycol dimethyl ether (2G, diglyme) as an additive. *Operando* X-ray diffraction and ex-situ ss-NMR techniques are employed comprehensively

to understand the co-intercalation reaction of these cyclic ethers, along with Na⁺-glymes, into graphite during cycling. When using these mixed electrolytes i.e., THF/2G and DOL/2G, the voltage profiles changes compared to the pure glyme-based electrolyte, while showing comparable specific capacities and good long-term durability. Overall, we propose that even trace amounts of diglyme prompt the co-intercalation of THF and DOL into graphite layers. This leads to the formation of quaternary graphite intercalation compounds (q-GICs), expanding beyond the realm of ternary graphite intercalation compounds (t-GICs).

1. Introduction

The development of energy storage, such as rechargeable batteries, becomes crucial as the world transitions away from fossil fuels. Especially, the increasing demand and attention towards lithium-ion batteries (LIBs) can be attributed to their

excellent electrochemical performance.^[1–3] Due to their chemical similarity with lithium, sodium-ion batteries (SIBs) are one of the promising candidates for an alternative rechargeable battery technology.^[4–6] Even though graphite shows widespread use in LIBs, its application in SIBs is restricted due to the unavailability of thermodynamically stable high-capacity binary graphite intercalation compounds (b-GICs).^[5,7] Theoretical studies of unstable Na-GICs can be found in the literature. For instance, Lenchuk *et al.* showed that Na-GICs are unstable regardless of the concentration of sodium atoms.^[7] Jache *et al.*, however, reported that the limitation of graphite as an electrode in SIBs can be mitigated by using linear ether-based electrolytes, where solvated ions enter the graphite galleries to form ternary graphite intercalation compounds (t-GICs).^[8]



The reaction was observed to be reversible, fast, and stable over even thousands of cycles. Despite the extensive research over the last decade, the electrochemical reaction with sodium has only been reported for different glymes (from monoglyme to pentaglyme and crown-ethers, as well as some glyme derivates) and sporadically the use of ethylenediamine as a co-solvent.^[9–11] There have been reports on various chemically prepared t-GICs using different solvents and alkali metals,^[12] although, the syntheses require elevated temperatures. Conversely, the exploration of electrochemical synthesis for these compounds remains untested, and intriguingly, in some cases, it has been shown to be non-reversible or unstable.^[13–17] Following a recent publication by us, showing that immediately

[a] Y. Son, Dr. G. Åvall, Dr. G. A. Ferrero, Dr. I. Escher, K. A. Janßen, Prof. Dr. P. Adelhelm

Institut für Chemie

Humboldt Universität zu Berlin

Brook-Taylor-Str. 2, 12489 Berlin, Germany

E-mail: philipp.adelhelm@hu-berlin.de

[b] Dr. G. Åvall, Dr. A. I. Freytag, Prof. Dr. P. Adelhelm

Research group Operando Battery Analysis (CE-GOBA), Department Spins in Energy Conversion and Quantum Information Science (SE-ASPIN)

Helmholtz-Zentrum Berlin

Hahn-Meitner-Platz 1, 14109 Berlin, Germany

[c] M. Jauregui, Dr. D. Saurel, Dr. M. Galceran

Centro de Investigación Cooperativa de Energías Alternativas (CIC energiGUNE)

Basque Research and Technology Alliance (BRTA)

Parque Tecnológico de Álava

Albert Einstein 48, 01510 Vitoria-Gasteiz, Spain

[d] M. Jauregui

Departamento de Física

Universidad del País Vasco

Aptdo. 644, 48080 Bilbao, Spain

 Supporting information for this article is available on the WWW under <https://doi.org/10.1002/batt.202300506>

 © 2024 The Authors. *Batteries & Supercaps* published by Wiley-VCH GmbH. This is an open access article under the terms of the Creative Commons Attribution License, which permits use, distribution and reproduction in any medium, provided the original work is properly cited.

when diethylene glycol dimethyl ether (2G, diglyme) solvated ions intercalate into graphite the interlayer spacing is turned into a slit pore which fills up with the free diglyme solvents of the electrolyte, it appears reasonable that once the slit pores are formed other, previously thought inert, solvents could enter the graphite structure.^[18] We therefore investigate whether small additions of diglyme to two different cyclic ether-based electrolytes, where previous attempts to electrochemically form a t-GIC has failed, can allow also the cyclic ethers to reversibly co-intercalate into graphite. Although several theoretical studies on the intercalation of Na^+ in graphite with cyclic ethers such as tetrahydrofuran (THF) and 1,3-dioxolane (DOL) have been conducted^[17,19], their experimental validation remains incomplete. In light of this, we present a re-evaluation of the utility of THF and DOL as primary solvents in the electrolyte. Both THF- and DOL-based electrolytes have shown low specific capacities ($< 30 \text{ mAh g}^{-1}$ and $< 10 \text{ mAh g}^{-1}$ respectively) which are typical of Na^+ b-GICs and make them a bad candidate for battery applications. Jache *et al.* found that THF co-intercalation takes place although with very low capacities and large voltage hysteresis, but that the poor initial specific capacity increases with the cycling (from 20 to 30 mAh g^{-1} over 50 cycles) which was ascribed to the activation process of the graphite due to the less favorable Na^+ -THF solvation complex.^[15] The reason for this low performance has not been clearly understood. On the one hand, Yoon *et al.* proposed that the solvation shell stability is not favorable for co-intercalation.^[17] Despite that, Au *et al.* successfully prepared such structures chemically.^[20] Yet a the pure THF-based electrolyte appears to be more or less electrochemically inert towards graphite. Additionally, DOL is also investigated as electrolyte solvent as it is, like THF, a member of the group of cyclic ethers. In contrast to THF, which has been studied for GIC using chemical and electrochemical methods, DOL received little attention so far; with the exception of Li-S and Li-O₂ batteries.^[21–23]

We show that electrolytes based on THF/2G and DOL/2G mixtures exhibit an improved reversible capacity of $\approx 90 \text{ mAh g}^{-1}$ (compared to the pure THF and DOL systems) after 500 cycles, already at very low amounts of diglyme (10 vol % or lower, i.e., at additive levels) with an altered voltage profile compared to pure 2G. In other words, this suggests that quaternary graphite intercalation compounds (q-GICs) form, i.e., GICs containing two different types of solvents as intercalants. The approach to mixing solvents to obtain q-GICs was recently demonstrated chemically and electrochemically by Zhang *et al.* and Escher *et al.* for solvent mixtures of diglyme and ethylenediamine.^[9,24] An intriguing effect of this dual solvent co-intercalation is that the undesired expansion of the graphite lattice can be significantly reduced as compared to when diglyme is used alone.^[9,24] Recently, Liang *et al.* reported on the successful use of DOL as a co-solvent in high voltage Graphite// $\text{Na}_3\text{V}_2(\text{PO}_4)_2\text{O}_2\text{F}$ full cells. DOL was found to offer high oxidative stability towards the cathode material, while remaining feasible for use with the graphite anode as well.^[25] In these studies, however, glyme has been the primary solvent ($> 90 \text{ vol\%}$). Therefore, it is not surprising that co-intercalation is observed,

and the voltage profile of Na//Graphite half-cells closely resembles that of a pure 2G-based electrolyte.

In contrast, in this work we focus on THF and DOL-based electrolytes and using very small amounts of 2G as electrolyte additive. We find that while THF is not able to co-intercalated on its own, it is able to do so once 2G is present in the system. Similar behavior is seen when THF is replaced by DOL. Therefore, 2G can work as an enabler for other solvents to reversibly intercalate and deintercalate into graphite. This way, quaternary graphite intercalation compounds (q-GICs) are formed, i.e., GICs containing sodium ions and two different types of solvents are intercalant. We investigate the graphite structure evolution during cycling using *operando* X-ray diffraction (XRD), and the electrode thickness variation by *operando* electrochemical dilatometry (ECD), while solid-state nuclear magnetic resonance (ss-NMR) is used to support the explanation of the co-intercalation mechanism of THF/2G electrolyte in the graphite structure. Finally, theoretical calculations on the electrolyte and solvated ions inside the graphite structure is used to support the findings.

Experimental Section

Cell Preparation

Graphite electrodes were prepared by mixing graphite powder (MTI Corp.) with polyvinylidene fluoride (PVdF, from PI-KEM Ltd) at a mass ratio of 9:1 in N-methyl-2-pyrrolidone (NMP, from Sigma-Aldrich) as solvent. The mixture was casted on carbon-coated copper current collector by doctor blade. The electrodes were punched out with a diameter of 12 mm of diameter and dried at 110°C under vacuum. The prepared electrodes have an active materials mass of $\approx 8\text{--}10 \text{ mg/cm}^2$.

The electrolytes were pre-dried overnight using porous molecular sieves (3–4 Å). Diglyme (2G, Sigma Aldrich), 1,3-dioxolane (DOL, Sigma Aldrich), and tetrahydrofuran (THF, Sigma Aldrich) were used with sodium hexafluorophosphate (NaPF_6 , purity $> 99\%$, E-Lyte) as conductive salt. Several electrolyte solutions were prepared by varying three factors: the molar glyme per salt ratio (2G/ NaPF_6), the molar carbon per glyme ratio (C/2G), and the molar THF per glyme ratio (THF/2G). DOL/2G electrolytes were prepared similarly as THF/2G electrolytes.

Electrochemical Measurements

Electrochemical measurements were carried out using CR2032 coin cells (MTI Corp.). The coin cells were assembled in an Ar-filled glove box ($\text{H}_2\text{O} < 0.1 \text{ ppm}$, $\text{O}_2 < 0.1 \text{ ppm}$). For the measurement of electrochemical properties, sodium metal (BASF) was used as the counter electrode and Whatman membrane (GF/A) as separator with 100 µl of electrolyte. For galvanostatic cycling tests, the assembled coin cells were cycled with 11 mA g^{-1} for five cycles in the potential range of 2.0–0.001 V versus Na^+/Na .

Cells for *operando* electrochemical dilatometry (ECD) were prepared in an Ar-filled glove box ($\text{H}_2\text{O} < 0.1 \text{ ppm}$, $\text{O}_2 < 0.1 \text{ ppm}$) with graphite electrode (diameter of 10 mm) and an active material mass loading of $\approx 6\text{--}7 \text{ mg/cm}^2$. The ECD cell (ECD- 3-nano by EL-CELL GmbH) provides a 3-electrode geometry, where sodium metal was used as both counter and reference electrode. The electrolyte volume employed in these cells was $\approx 250 \mu\text{l}$. Before cycling, the

cells were rested in the climate chamber for 6 hours to equilibrate. The thickness changes were recorded continuously during galvanostatic charging-discharging at 11 mA/g. The thickness change (%) was calculated by the following equation:

$$h_{\text{relative}}(\%) = \frac{h_n}{h_0} \times 100 \quad (2)$$

Where h_n is the electrode thickness at each time without the thickness of the current collector and h_0 is the initial thickness of the electrode without the thickness of current collector after 4 hours of OCV. A detailed explanation of the method can be found here.^[9]

Material Characterization

Operando X-ray powder diffraction (XRPD) measurement were performed on a Lab-scale Bragg-Brentano diffractometer (Bruker D8 Advance with Cu K- $\alpha_{1,2}$ tube source and LYNXEYE 1D detector), using CIC energiGUNE's custom made *in-situ* electrochemical cell equipped with a Beryllium window; see Saurel *et al.*^[26] for more details on the cell characteristics). The galvanostatic cycling during the *operando* XRPD experiment were controlled by a Bio-Logic SP-150 potentiostat. Graphite electrodes with a diameter of 14 mm were prepared by casting an N-Methyl-2-pyrrolidone (NMP) based slurry through a mask directly onto the cell's Beryllium window. The slurry composition was 95:5 in graphite powder and Polyvinylidene fluoride (PVDF) binder, respectively; no carbon black additive was added. The electrochemical cell was assembled in an Ar-filled glove box ($H_2O < 0.1$ ppm, $O_2 < 0.1$ ppm) using a Whatman membrane (GF/A) as separator with 140 μ l of electrolyte.

Solid-state NMR Hahn-echo experiments were performed at room temperature on a Bruker 400DNP Ascend (^{23}Na and ^{13}C Larmor frequencies of 105.86 and 100.63 MHz, respectively). 4 mm zirconia rotors were spun at 10 kHz. 1 M NaCl (0 ppm) was used as a reference for ^{23}Na and adamantane powder for ^{13}C (29.46 ppm).^[27] Further information on the experimental NMR parameters can be found in Table S2 of the Supporting Information. Samples for ex situ Magic Angle Spinning (MAS) ss-NMR were prepared by disassembling the cycled coin cells under argon atmosphere and filling the rotor with the graphite powder and electrolyte-soaked glass fiber separators from the coin cell. Only the sodium counter electrode was discarded before sample-packing as it would prevent the sample holder from rotating in the magnet.

Theoretical Calculations

Solvation shells with two 2G molecules, one 2G and three THF, and six THF molecules, as well as a single 2G and THF molecule, were constructed and optimized using the Gaussian 16 suite.^[28] The B3LYP functional was used alongside the 6-311+ +G(d,p) basis set.^[29-31] Furthermore an implicit solvent was used through the SMD model, with dielectric constants set to 7.23, 7.6, and 7.6, respectively, for the 3 solvation shells, and Grimms empirical dispersion was included.^[32-33]

The three solvation shells were placed inside the interlayer spacing of expanded graphite composed of 50 carbon atoms, and the structures were optimized using the Vienna ab initio package (VASP).^[34-38] A 6x6x6 Gamma centered k-point mesh was used alongside the PBE functional and a plane wave cut-off of 520 eV was used.^[39]

Car-Parrinello molecular dynamics was used to investigate the solvation shells in two electrolytes^[40]: A standard electrolyte with a

2:1 2G:salt ratio and 1:10 2G:THF ratio electrolyte (four NaPF_6 , eight 2G, forty THF, approximately 0.9 M salt concentration and 73 vol% THF), representing an electrolyte where it is possible to fully solvate Na^+ with only 2G, and a 2G deficient electrolyte with 0.5:1 2G:salt ratio and 1:10 2G:THF ratio electrolyte (eight NaPF_6 , four 2G, forty THF, 2.1 M salt concentration, 85 vol% THF), representing an electrolyte where it is not possible to fully solvate Na^+ with only 2G. The PBE functional was used with a plane-wave cut-off of 90 Rydberg and a time step of 4 a.u.^[39] The initial structures were generated with packmol with all molecules and ions randomly distributed in the periodic box. After equilibration, a Nosé-Hoover thermostat was switched on to keep the temperature at 300 K, and subsequent production runs of 20 ps were carried out. From the trajectories the (partial) radial distribution functions (RDFs) were calculated as

$$g_i(r) = \frac{n_i(r)}{4\pi r^2 \Delta r \rho_i} \quad (3)$$

where $n_i(r)$ is the average number of atoms of species i in a spherical shell with thickness Δr at distance r from the Na^+ , and ρ_i is the average number density of atom i . The partial coordination numbers were calculated by integrating the (partial) RDFs, the (partial). The solvation number was computed similarly by replacing solvents by their center of mass and computing the Na^+ -CM partial RDFs, as described elsewhere.^[41]

2. Results and Discussions

2.1. Electrochemical Characterization

Figure 1a) compares the voltage profiles for cells with THF, 2G and the THF/2G mixture as electrolyte solvent. In all cases, NaPF_6 is used as conductive salt. In line with our earlier findings,^[15] the pure THF-based electrolyte leads to very low capacity values and ill-defined voltage profiles. The decrease on the discharge capacity from $\approx 50 \text{ mAh g}^{-1}$ in the first cycle to less than 20 mAh g^{-1} in the second cycle indicates that the processes are largely irreversible and side reactions occur. The small reversible capacity might be due to the formation of high stage b-GICs (NaC_{64} corresponds to 35 mAh g^{-1}) although one would expect a more defined voltage profile in this case. Similarly, in the pure DOL-based electrolytes very low capacities, typical of sodium b-GICs are observed (see Figure S2). Thus, neither THF nor DOL show any propensity for electrochemical solvent co-intercalation, even though t-GICs with both solvents can be chemically prepared.^[15,17] In contrast, 2G-based electrolytes are the most well studied case for which sodium t-GICs are formed, showing capacities of $\approx 110 \text{ mAh g}^{-1}$.^[8,16]

By adding small amounts of 2G to a THF-based electrolyte (THF/2G=8:2 v/v%), 90 mAh g^{-1} of discharge capacity is observed in the first cycle, Figure 1a). This is not surprising as the ions solvated by 2G molecules should be able to co-intercalate and form t-GICs. However, unexpectedly, the voltage profile changes drastically – the main voltage plateau observed at 0.65 V (vs. Na^+/Na) in 2G-based electrolytes drops to 0.45 V and an additional plateau at 0.15 V appears, indicating that a secondary electrochemical reaction occurs for the solvent

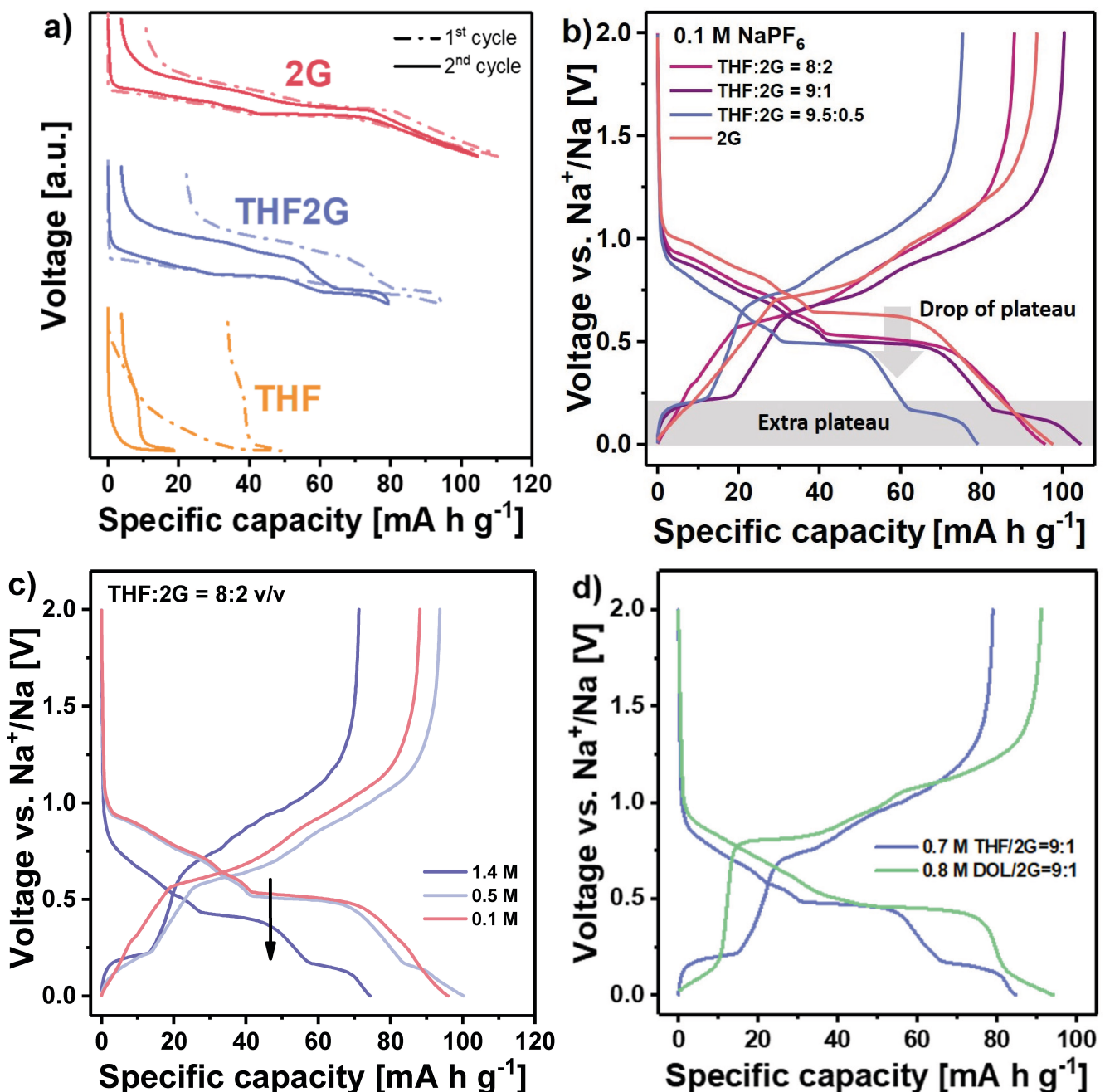


Figure 1. Voltage profiles for graphite electrodes in different electrolytes a) Hysteresis plot of (1st and 2nd cycles) of graphite half cells with 1 M NaPF₆ in 2G and THF:2G = 8:2 electrolyte (1.4 M NaPF₆), and 1 M NaPF₆ in THF and b) voltage profiles with different ratio of THF:2G solvent at 0.1 M (in the same salt concentration) (2nd cycle) c) voltage profiles with different concentration of salt in THF:2G = 8:2 electrolyte d) voltage profiles of THF:2G = 9:1 electrolyte and DOL:2G = 9:1 electrolyte (2nd cycle). (All mentioned ratios refer to volumetric ratio and these measurements were performed at 11 mA g⁻¹)

mixtures. While 2G obviously supports the co-intercalation of THF, it is unclear how much 2G is needed to enable this effect.

For a more systematic evaluation of the observed behavior, we decided to limit the amount of 2G in relation to the amount of conductive salt in two ways: *i*) keeping the amount of salt constant but reducing the amount of 2G while increasing the amount of THF, *ii*) keeping the amount of 2G and THF constant while increasing the salt concentration. It should be highlighted, however, that not only the ratios between solvents and salts can have an important influence on the electrochemical

behavior, but also their relation with the active mass of the graphite electrode. For instance, the same electrolyte can show either a voltage profile similar to a pure 2G-based electrolyte with a single voltage plateau, when there is a large amount of 2G molecules per active mass, or one with two plateaus, when there are few 2G molecules per active mass, see Figure S1. Thus, a constant mass loading of 8–10 mg/cm², and a fixed total electrolyte volume of 100 µl are used to ensure that the effects seen are due to the electrolyte composition. Several NMR studies have indicated that at full sodiation, there are both free

and bound solvents inside the graphite galleries, and a recent paper by Escher *et al.* indicate that there are 2–3 2G molecules per Na^+ in the graphite at full sodiation.^[18,42] This would indicate that roughly 1.2–1.8 μl of 2G is needed per mg of graphite. Thus, an electrode with a radius of 12 mm and a loading of 9 mg/cm^2 requires in the range of 12–18 μl of 2G at full sodiation. However, even more 2G is required to reach full sodiation as measurement indicate that the largest amount of 2G in the system occurs on the main voltage plateau, after which there is a decrease of solvent molecules in the graphite.^[18] Thus, 100 μl of electrolyte with less than 10 vol% 2G should not be able to fully sodiate such an electrode.

Starting with the first approach, *i*) when the volume of 2G in the cell is varied from 20% to 5% total solvent volume, while maintaining a molar concentration of 0.1 M, the main voltage plateau shifts to lower potentials while a similar full capacity of over 100 mAh g^{-1} is reached (see Figure S1), typical of systems with only 2G. With 10% and 5% 2G, however, a second voltage plateau is observed at 0.15 V vs. Na^+/Na , which might indicate that ions not fully solvated by 2G are participating in an additional reaction. The amount of 2G in the 10% and 5% electrolyte solution is not enough to sodiate the graphite. Thus, the reaction should stop when the system runs out of 2G molecules. In such a glyme restricted setup when the amount of 2G is cut in half, i.e., going from 10 vol% to 5 vol% 2G, the capacity should be cut in half. Yet this is not observed, (109 mAh g^{-1} for 10 vol%, 92 mAh g^{-1} for 5 vol%) indicating that not only 2G is participating in the reaction.^[18] This strongly indicates that not only 2G, but also THF, is taking part in the reaction to sodiate the graphite.

For the second approach, *ii*) as can be seen, Figure 1c), THF/2G=8:2 with a 0.1 M salt concentration shows a voltage profile typical of a pure 2G-based electrolyte. However, when increasing the salt concentration, the voltage plateau at 0.65 V vs. Na^+/Na again drops with the appearance of the second plateau at 0.15 V vs. Na^+/Na .

Thus, both methods *i*) and *ii*) that limit the number of cations fully solvated by 2G lead to similar results, and similar effects are seen for a large variety of salt and solvent ratios, (see Figure S1). We extended the same methodology with the addition of small amounts of 2G to a DOL-based electrolyte and a similar effect is observed. The voltage profile of the DOL/2G=9:1 electrolyte is different from the pure 2G-based electrolyte, as well as the THF/2G=9:1 electrolyte, Figure 1d) and S2. The main plateau is again located at ≈ 0.45 V vs. Na^+/Na , similar to the THF-based electrolyte, however, the DOL-based electrolyte enables a larger specific capacity of $\approx 80 \text{ mAh g}^{-1}$ at the end of the plateau. Last but not least, unlike the THF-based electrolyte, the DOL-based electrolyte shows no defined additional plateau at 0.15 V vs. Na^+/Na but instead a change of the slope between 0.14 and 0.001 V vs. Na^+/Na . The different voltage profiles between THF- and DOL-based electrolytes indicate that both solvents participate in the electrochemical reaction, even if they are unable to do so without 2G present in the system. This altered electrochemical behavior is attributed to the co-intercalation of both 2G and THF/DOL, resulting in the formation of quaternary GICs. The mixtures containing THF and

DOL exhibit different voltage profiles, indicating that the electrochemical performance is dependent on all the solvents, and their ratios, present in the electrolyte. The fact that several solvents jointly co-intercalate into the graphite structure suggests that likely many more q-GICs (or even higher order GICs) exist that are not explored to date.

Differential capacity plots show clear differences between the pure 2G electrolyte and THF/2G electrolyte (shown in Figure S3). Notably, during sodiation the first maximum is shifted to lower potentials at 0.48 V vs. Na^+/Na . The observation aligns with previous finding of a small peak at 0.15 V vs. Na^+/Na for a pure 2G electrolyte, which is attributed to an in-plane superstructure indicated by XRD data.^[43] It seems that the additional co-intercalation of THF promotes the formation of this in-plane superstructures and renders it more distinguishable. Overall, these electrochemical measurements show that the modification of the electrolyte composition can alter the mechanism of the reaction in which other solvent electrolytes (THF and DOL) are now participating in the sodiation reaction.

At this point, one might wonder whether THF is unable to co-intercalate into pristine graphite due to a combination of a larger solvation shell (compared to 2G)^[44] and the fact that the structure has not yet expanded, or that 2G acts as a facilitator for the THF, ultimately allowing both solvents to co-intercalate. To elucidate the electrochemical mechanism in the THF/2G electrolytes, we performed galvanostatic cycling with a 2G-based electrolyte that was later replaced by a THF-based electrolyte. Thus, after cycling the graphite electrodes in 1 M NaPF_6 in 2G, the cell was stopped at the desodiated state (2.0 V vs. Na^+/Na), and the graphite electrodes were recovered in an Ar filled glovebox. Then, the cycled graphite was washed several times with THF and dried overnight (at room temperature in the glove box). Finally, the dried graphite electrode was re-assembled in a fresh cell with 1 M NaPF_6 in THF and sodiated once again. As shown in Figure 2a), the first cycle shows a specific capacity $\approx 80 \text{ mAh g}^{-1}$, and then maintained a capacity of $\approx 50 \text{ mAh g}^{-1}$ in subsequent cycles, which is higher than if the cell was never pre-cycled in a pure 2G electrolyte. Nevertheless, the voltage profile appears more similar to those reported for hard carbon materials which can be ascribed to the increased surface area due to the expansion of the carbon lattice upon solvent co-intercalation with 2G.^[11,45] Using the same process, a cell was cycled with a 2G-based electrolyte but now stopped at a potential where solvated ions are still present in the graphite (at 0.7 V vs. Na^+/Na). The cell was opened, and the graphite electrode went through the same procedure as described, but only dried for a short time to remove the excess THF, and finally re-assembled into a fresh cell with a pure THF electrolyte showing the same voltage profile as a THF/2G electrolyte, which demonstrated that the remaining diglyme-solvated ions already inside the graphite influence the electrochemical behavior in the THF-based electrolyte (see Figure 2b)). This is in agreement with the pore formation model previously proposed by us, where a t-GIC formed using diglyme should act as a slit pore which free solvents can enter.^[18] From these experiments it can be inferred that a minuscule amount of 2G solvated ions in the graphite layer is sufficient to enable further

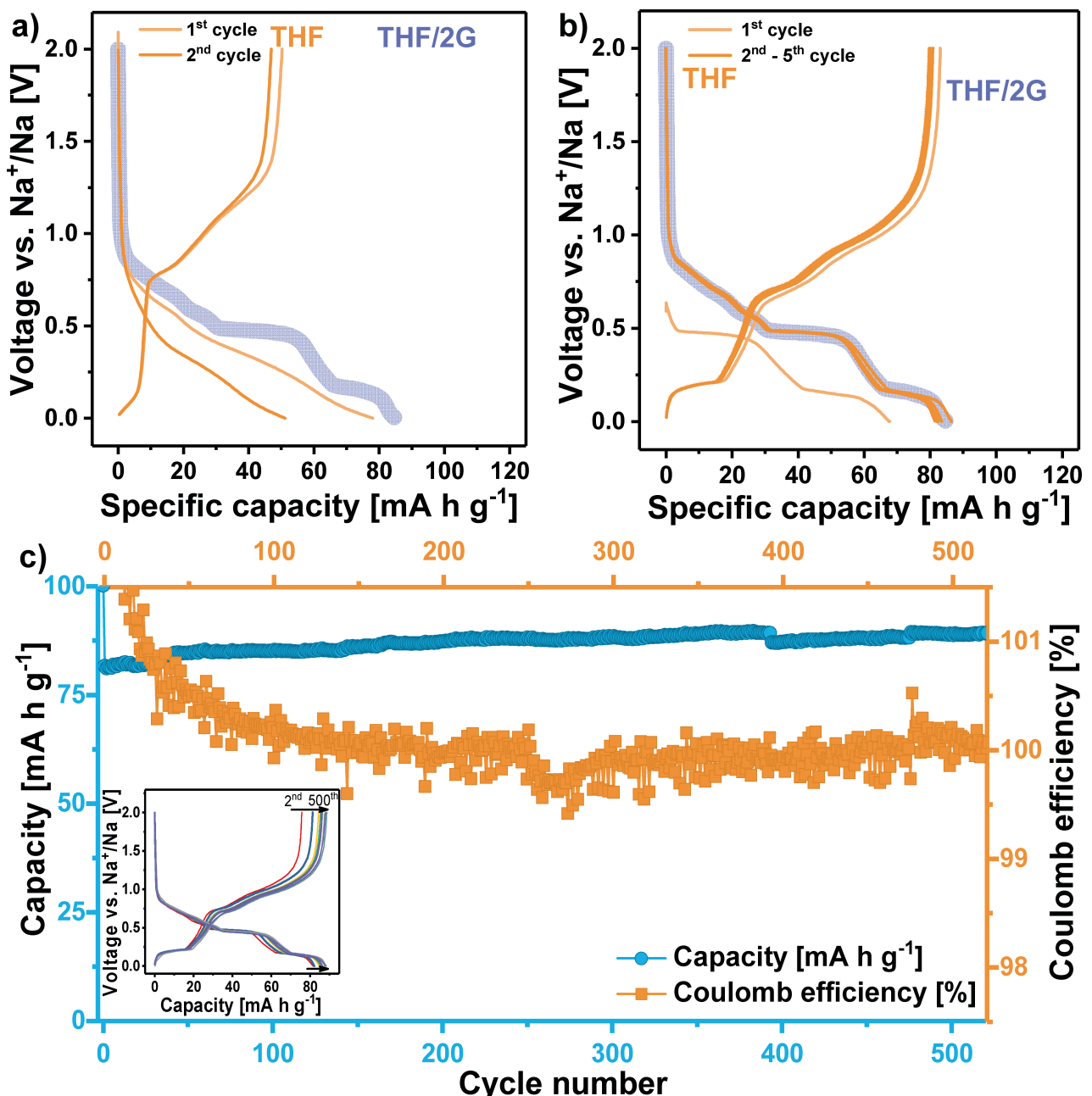


Figure 2. Effect of pre-cycling on the voltage profile of graphite electrodes in THF-based electrolytes and long-term cycling measurement a) voltage profile of graphite electrode using a THF electrolyte. Before cycling, the cell was pre-cycled for one cycle in a 2G electrolyte and stopped at 2.0 V, i.e., desodiated state. b) voltage profile of graphite electrode using a THF electrolyte but pre-cycling and stopped at 0.7 V, c) cycle life test for a 1.4 M THF/2G=8:2 electrolyte, and voltage profiles of 2nd, 50th, 100th, 150th, 200th, 300th, 400th, and 500th cycles by 22 mA g⁻¹. All electrolytes contained 1 M NaPF_6 . For comparison, graphs a) and b) also show the voltage profile of the graphite electrode when cycling in THF/2G electrolyte (purple)

co-intercalation with THF molecules. Even the desodiation of 2G solvated ions seems to activate the graphite to allow THF solvated ions to co-intercalate. Overall, the results clearly show that diglyme acts as a “gate opener” enabling or facilitating the co-intercalation of THF solvated sodium ions to form q-GICs.

Figure 2c) shows long-term cycling results for a cell with 1.4 M NaPF_6 in THF/2G=8:2 as electrolyte. According to the result of rate capability, a relatively modest current value of 22 mA g⁻¹ was set (see Figure S4). Therefore, long-term cycling was conducted gradually, spanning a total of 21 weeks. The

initial Coulomb efficiency amounts to 73 % indicative for some side reactions. Afterward, following 500 cycles, the system achieves an average Coulomb efficiency of 100% during the last 100 cycles, coupled with a capacity of 89.3 mAh g⁻¹. The inset shows the voltage profiles for selected cycles which show the stability of the electrode in this electrolyte mixture. Thus, this new electrolyte composition with a different electrochemical mechanism exhibits an excellent stability over several cycles.

2.2. Structural Characterization of Graphite Electrode in THF/2G Electrolyte

2.2.1. Operando X-ray Diffraction

To study the structural evolution of the graphite electrode in the THF/2G electrolytes, *operando* X-ray diffraction (XRD) was conducted. Figure 3a) shows the results of the *operando* XRD measurement of graphite with THF/2G=8:2 electrolyte in during the 4th cycle. As can be observed, the *operando* XRD

measurements indicates that the graphite electrode undergoes staging with the splitting of the (002) peak into two peaks and the appearance of new features at around 15° at higher states of sodiation. This behavior was already observed with a pure 2G electrolyte.^[43,46] These peaks disappear upon desodiation, indicating that the formation of these structures is reversible. However, a small peak, or a shoulder on the most intense peak, towards lower angles is always visible, indicating the presence of different solvation shells inside the structure. Looking at the diffractogram of the fully sodiated system and comparing it

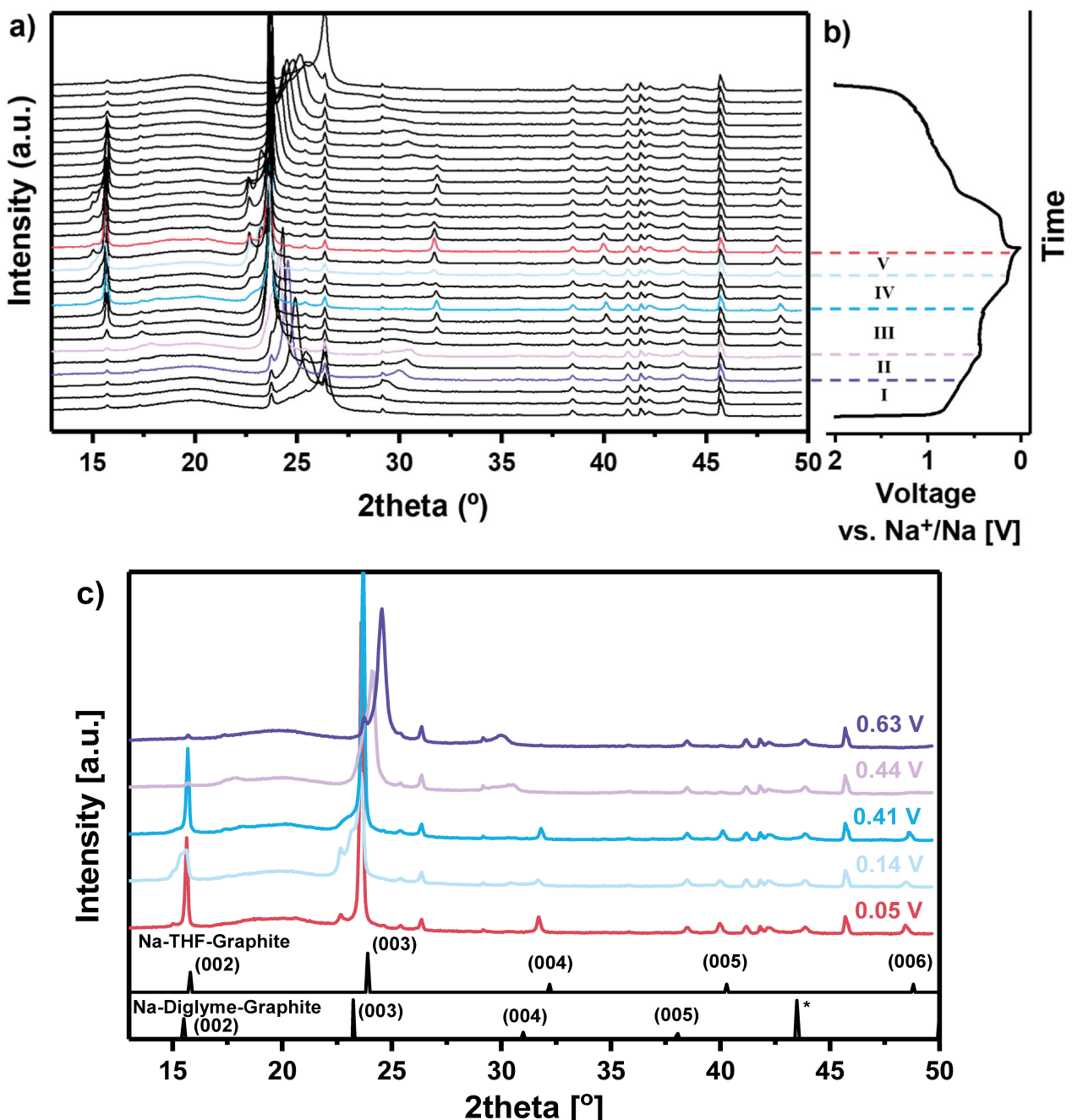


Figure 3. Structure evolution during cycling (4th cycle) a) Results from *operando* X-ray diffraction of sodium ion intercalation/deintercalation into graphite in THF/2G electrolyte (1.02 M THF/2G=8:2) ($\text{CuK}\alpha = 1.542 \text{ \AA}$), b) with the corresponding voltage profile, and c) selected diffraction patterns during discharging. The peak marked with an asterisk is due to the copper current collector. The data for the Na-THF-Graphite and Na-Diglyme-Graphite is taken from Au *et al.*^[20] and Goktas *et al.*^[11].

with the fully sodiated graphite in a diglyme-based electrolyte, and the fully sodiated chemically prepared THF t-GIC as reported by Au *et al.*, the most intense peak is close to the THF-based compound (23.9° vs. 23.62° in our case), while the less intense peak can be ascribed to the diglyme compounds.^[15,20,43] This indicates that THF is present in larger amounts than diglyme in the fully sodiated state. Taking the angle of the most intense peaks (23.62°) we calculate an interlayer distance of 11.3 \AA , which is less than what is observed when a diglyme-based electrolyte is used.^[43,46] The finding of a smaller expansion is in line with the dilatometry results presented in the next section.

The occurrence of a second feature in the XRD pattern suggests that the presence of THF causes the formation of additional intercalation compounds, i.e., ternary and/or quaternary intercalation compounds. One might wonder about the possibility of an incomplete sodiation that gives the result to a partial mix of stage I and II as a result of the existence of both peaks in the 22.6° – 23.6° range. However, we can discard this possibility due to the existence of all the peaks previously mentioned and detected by Au *et al.*, in addition to the peaks located at 40.04° (and not at around 38° where 2G exhibited an additional peak) and 48.5° . We can infer from these results that the THF/2G-based electrolyte exhibits an XRD pattern with new graphitic co-intercalation compounds that are produced electrochemically and with a smaller lattice expansion compared to the pure 2G-based electrolyte.

2.2.2. Operando Electrochemical Dilatometry (ECD)

The expansion of the graphite interlayer distance leads to a macroscopic expansion of the electrode, which can be studied by electrochemical dilatometry (ECD).^[47] ECD measurements were conducted with an electrolyte composed of 1 M NaPF_6 in 2G, as well as 0.5 M of $\text{THF}/2\text{G}=9.5:0.5$ electrolyte. Results are displayed in Figure 4 and show that the electrode expansion is notably smaller for the solvent mixture (119% vs 175%). The fact that the electrode expansion can be reduced by addition of a co-solvent was previously observed by Escher *et al.* for the addition of ethylenediamine (EN2 N) to 2G. However, the addition of THF to the electrolyte seems to reduce the thickness expansion even more than the addition of EN2 N (see Figure S5). In view of practical batteries, changes in the electrode thickness during battery charging/discharging should be small in order to avoid mechanical problems. The use of co-solvents therefore appears an attractive strategy to mitigate the quite large lattice changes typically observed for solvent co-intercalation reactions.^[9] The effect is also preserved during cycling, i.e., the expansion/shrinkage of the electrode over several charge/discharge cycles ("breathing") decreases from 46% (2G) to 32% (THF/2G) (see Figure S5).

While the ECD measurements provide valuable *operando* data, it is important to realize that in the special cell setup, the electrode capacity is often slightly lower as compared to the standard coin cells. We, therefore, compare not only the thickness change with other electrolytes but also the derivative

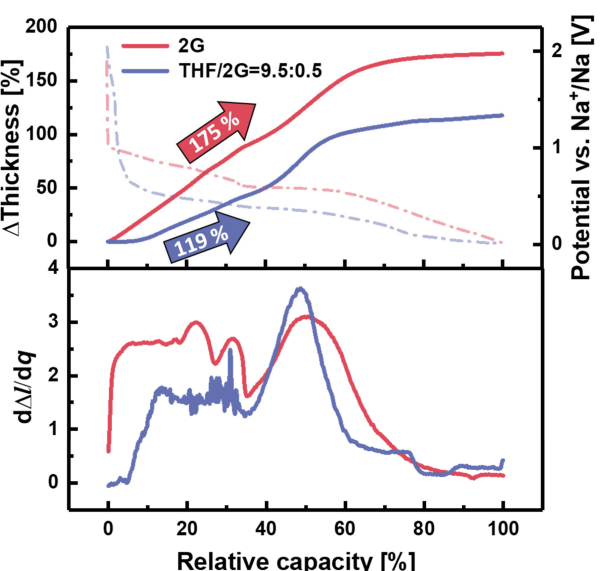


Figure 4. Results from *operando* electrochemical dilatometry. Change in electrode thickness ($\Delta\text{Thickness}$) during sodiation of graphite electrodes using a 2G-based and a THF/2G-based electrolyte (both 1 M NaPF_6 , first cycle). The bottom graph shows the corresponding derivative plots ($d\Delta/\Delta q$).

data, for a better comparison of the systems when their capacities differ.^[9,47–48] The derivative plot (thickness change vs. relative capacity) shows a larger increase at the beginning of the process for the pure 2G electrolyte, that can be ascribed to the higher intake of free 2G molecules (flooding) as demonstrated recently by Åvall *et al.*^[18] In the case of the THF/2G mixture, this increase, although existing, is less intense. In addition, the measurement with the THF/2G electrolyte exhibits a sharper peak around the plateau region, indicating that the expansion at this point occurs faster than using pure 2G. Furthermore, there are two other peaks below 50% that are not visible in the case of the THF/2G mixture which suggest that staging mechanism observed in the case of 2G is less visible as a result of the lower amount of this solvent. Finally, at lower voltages, the derivative plot exhibited a change that coincides with the presence of the second additional plateau, and that it is not visible in the 2G electrolyte system. Overall, the findings clearly proof that the sodiation mechanism changes when adding THF to the 2G electrolyte with a smaller thickness electrode expansion, although with a similar breathing effect.

2.2.3. Ex Situ Solid-State NMR Spectroscopy

To compare differences in the co-intercalation process, ^{23}Na and ^{13}C MAS NMR spectra were collected at the sodiated state (0.01 V) for the various solvent configurations as shown in Figure S6a) and Figure 5a). It is evident from the ^{23}Na data that 2G shifts the NMR signal to higher frequencies indicating a stronger solvent effect than for THF.^[49] Interestingly, the mixture of THF/2G shows a multitude of signals, which some authors assigned as NaPF_6 salt degradation.^[50] Nevertheless, the fact that long-term cycling is possible (see Figure 2c), suggests that

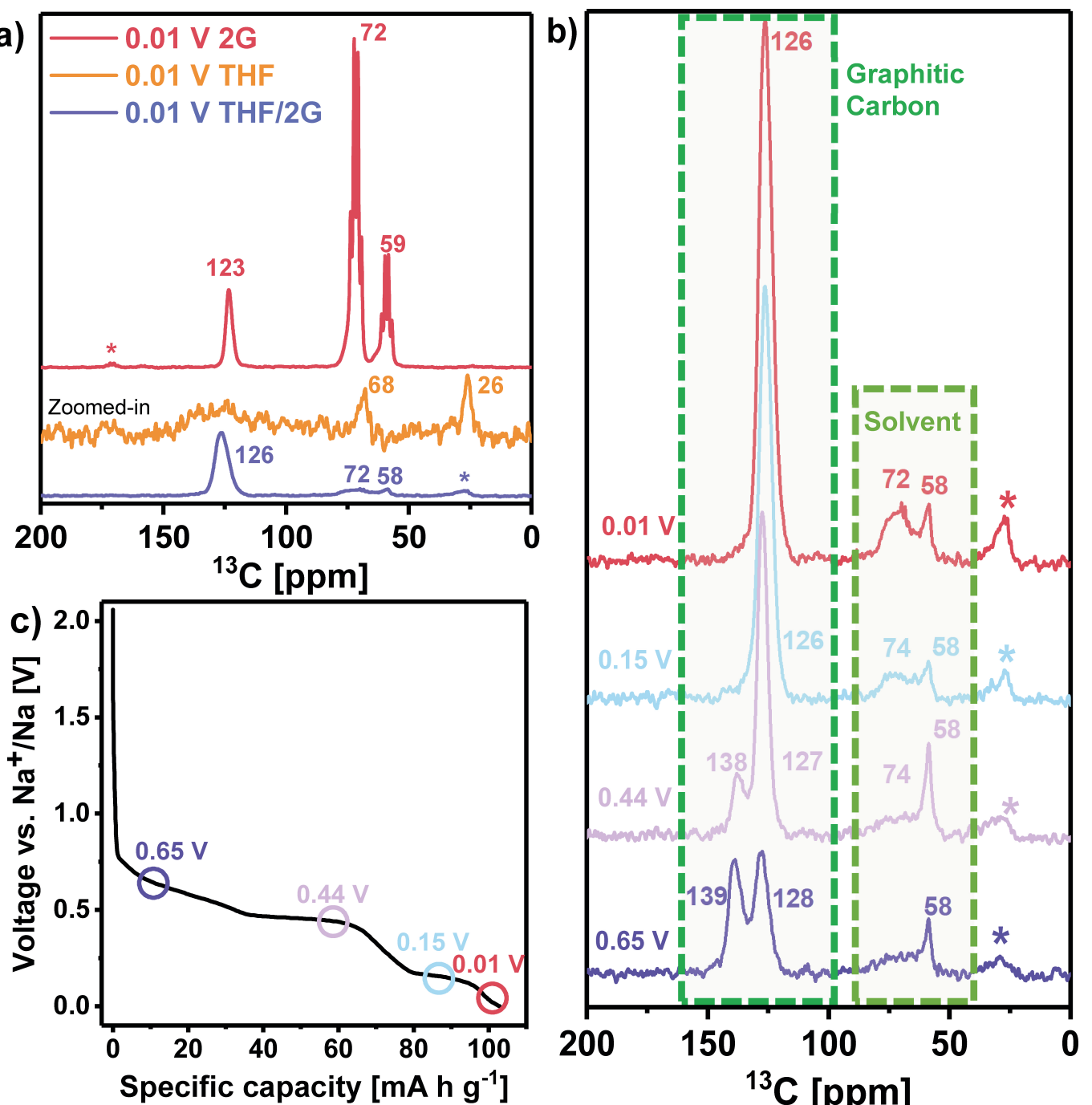


Figure 5. Results from ss-NMR measurements a) ^{13}C MAS NMR spectra of cycled samples at full sodiation for different solvent (2G, THF, THF/2G) configurations b) ^{13}C MAS NMR spectra of cycled samples for 0.7 M THF/2G = 9:1 electrolyte at different points on the discharge curve. Asterisks indicate spinning sidebands. Samples were normalized to their mass of active material. c) The first discharge curve of 0.7 M NaPF_6 in THF/2G = 9:1 electrolyte.

salt or electrolyte degradation seems a minor problem. No indication of a separate ^{23}Na signal for co-intercalated sodium ions for pure THF and 2G is apparent, which is different from previous co-intercalation studies.^[42,51–52] Note that the weak intensity of the spectrum for the THF electrolyte sample is related to the high vapor pressure of THF.

The ^{13}C NMR data in Figure 5a) confirms that co-intercalation is occurring in the 2G-based electrolyte and in the THF/2G

electrolyte although restricted in the pure THF. The signal at 123–126 ppm is assigned to the graphitic carbon adjacent to a solvated sodium ion layer in agreement with previous studies.^[42,51] The decrease in line width for the THF/2G electrolyte compared to pure 2G indicates a loss in mobility for the THF/2G electrolyte, which corroborates its lower rate capability (see Figure S4). This is pushed to the extreme for pure THF, where only a very broad peak is visible in the same graphitic

carbon region. The signals at 72 ppm and 59 ppm are assigned to the CH_2 and CH_3 groups of 2G, respectively. The THF signals at 68 ppm and 26 ppm are visible in the pure THF sample but not the THF/2G sample which can be ascribed to fast evaporation of THF solvent during NMR sample packing. For the pure 2G sample, very strong 2G solvent signals are apparent, with underlying broad peaks indicating the co-intercalated solvent species. Interestingly, for the mixture of THF/2G no free solvent is visible in the ^{13}C NMR spectrum, and the co-intercalated signals are much broader. This indicates a great loss of mobility of the co-intercalated 2G solvent in the presence of THF, consistent with a less expanded structure and hence more confined solvation shells, and a lower electrolyte conductivity compared to a pure 2G-based one. The 2G signal in the THF/2G sample shows an interesting feature, where only the signal for CH_2 (72 ppm) seems to be broadened but not the CH_3 signal (58 ppm).

To investigate this further, ex-situ samples of THF/2G electrolyte at different points on the discharge curve were analyzed as shown in Figure 6b) and Figure 5b). The ^{23}Na NMR data shows similar features throughout discharge. However, at high levels of sodiation (0.15 V and 0.01 V) a broad peak appears at -30 ppm, which may be attributed to sodium ions adsorbed to the graphite surface or irreversibly trapped inside the graphite,^[51] which can explain the irreversible capacity observed after the first cycle (see above, Figure 1a)).

In the ^{13}C NMR data (Figure 5b), at low sodiation levels a peak splitting in the graphitic region (126–139 ppm) is present, similar to pure 2G solvent as shown by Escher *et al.*^[42] This peak-splitting is still not fully understood as it appears in physically dried-out samples but also during the co-intercalation process. Clearly, a change in the solvation shell or the graphene stacking at these potentials are possible reasons for this peak split. Interestingly, these two peaks remain visible at lower voltage potentials (0.44 V) whereas this split disappears in the case of pure 2G below 0.625 V (see study by Escher *et al.*^[42]), which can be ascribed to the shifting of the main voltage plateau. In the solvent region (74 ppm and below) a sharp resonance at 58 ppm is visible in all spectra, which can be attributed to the CH_3 groups of 2G. However, the matching CH_2 peak (at a 2:1 ratio for 2G) is extremely broadened which may be due to a severe loss in mobility of the CH_2 chain in 2G that does not affect the mobility of the CH_3 group. However, due to the ensemble of peaks in the ^{23}Na NMR (Figure S6b), it can also not be excluded that some sort of degradation reaction occurred between 2G and THF and the ^{13}C NMR peak at 58 ppm stems from a degradation product. At 0.01 V some free THF solvent is visible, indicating a potential release of THF at low sodiation levels. This result can be understood with the new model for the solvent co-intercalation reaction proposed by Åvall *et al.*^[18] Once the first solvated ions (in this case, Na^+ -diglyme) are intercalated, the graphite structures open, allowing free solvents to enter the graphite structure. During further sodiation, the amount of free solvent molecules (mostly of THF) reduces as these molecules are replaced by solvated ions. To conclude, NMR experiments have demonstrated that the THF/2G-based electrolyte exhibited a co-intercalation mechanism

unlike the one observed in pure THF. However, this electrolyte exhibited a lower mobility compared to the pure 2G which is in agreement with the rate capability results.

2.3. Theoretical Considerations on the Graphite Electrode in THF/2G Electrolytes

The electrolyte, and the solvation shell in particular, has been identified as one of the major factors that determine if solvent co-intercalation occur.^[17–18,44] Several of the above tested electrolytes have a low absolute content of 2G solvents, making it impossible to fully sodiate the graphite using solvation shells with 2G molecules. However, the solvent to salt ratio is also a parameter of interest as it determines whether there are enough glyme molecules available to solvate the sodium ions. Even if there is enough glyme in the system to fully sodiate the graphite, there might be very few 2G molecules per Na^+ , making it very unlikely to find them in the solvation shell. Ab initio molecular dynamics of the standard electrolyte and the 2G deficient electrolyte (defined in the method section) shows an Na^+ coordination number of six, or slightly lower, in line with many previous studies, Figure 6a).^[41,53–62] Moreover, in both electrolytes anions are present in the solvation shell, in line with the poor conductivity and kinetics observed in these electrolytes. However, the standard electrolyte has more ion-aggregates while the 2G deficient electrolyte shows ion-pair formation, Figure 6a,b), in line with the higher salt concentration of this electrolyte. But the clearest difference between these electrolytes is the amount of 2G present in the solvation shell. While THF/2G electrolyte has both THF and 2G present in the solvation shell, the 2G deficient electrolyte barely has any 2G molecules present in the solvation shell, see Figure 6b). This means that it is rare to find solvation shells that are able to open up the graphite structure.

Optimizing three representative solvation shells (consisting of either two 2G molecules, one 2G and three THF molecules, or six THF molecules) inside the interlayer spacing, (Figure S7a–c), shows that the structure only containing 2G solvents is the most stable one, followed by the mixed solvation shell structure, while the one with six THF solvents is the most unstable, there being about 2.0 eV difference in formation energy between them. Hence, as the structures with solvation shells of only 2G molecules is the most stable it should form at a higher potential vs. Na^+/Na , compared with the others. This is in line with the observed electrochemical data as the voltage profiles, Figure 1b,c) and S1, the onset of sodiation is roughly 1 V vs. Na^+/Na , the same as in a pure 2G-based electrolyte, indicating that the sodiation process is initiated by the intercalation of solvation shells composed of only 2G molecules, while any formation of structures containing THF happens at lower potentials vs. Na^+/Na , which is also where the voltage profile shows the largest differences compared to a 2G-based electrolyte. This indicates that at high potentials mainly solvation shells with 2G solvents are intercalated, while the features observed at lower potentials are due to intercalation of solvation shells with THF present.

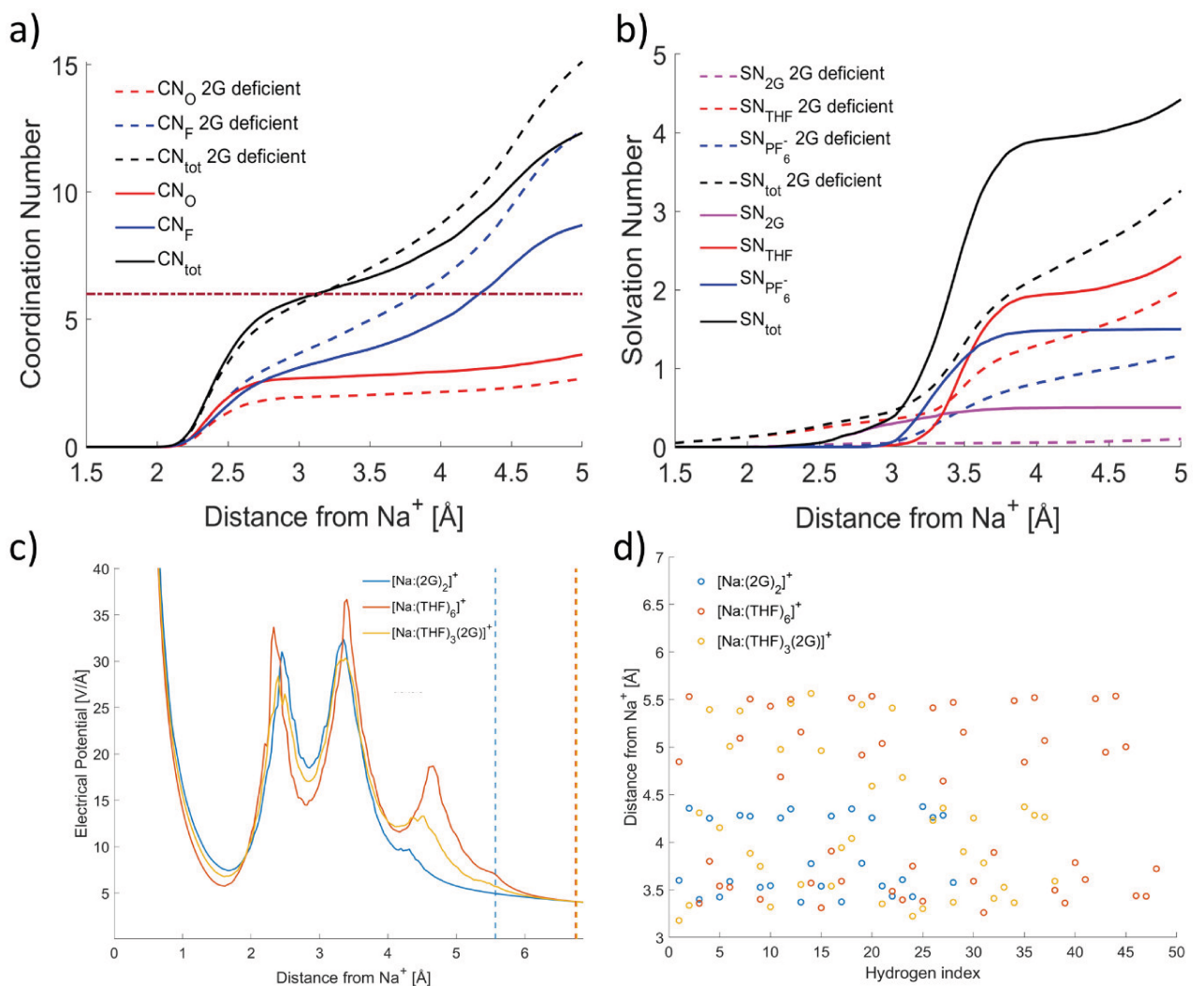


Figure 6. a) Coordination numbers and b) solvation numbers computed from the ab initio molecular dynamics simulations, c) the average electrical potential computed from the B3LYP optimized structures (radius of solvation shell marked in same color but dashed line) d) as well as the distances between the hydrogen atoms on the solvents and the Na^+ .

The size, solvation free energy, and electric potential outside the solvation shell has all been identified as crucial parameters for reversible solvent co-intercalation, hence these properties were computed for three selected solvation shells ($[\text{Na}:(2\text{G})_2]^+$, $[\text{Na}:(\text{THF})_3(2\text{G})_2]^+$, $[\text{Na}:(\text{THF})_2]^+$, Figure 6c-d).^[17–18,44] Although the solvation shell containing only 2G molecules is the smallest and most stable one, and hence the most prone to solvent co-intercalation, the THF containing solvation shells are surprisingly similar. The three studied solvation shells are all much smaller and more stable than, for instance, a solvation shell with propylene carbonate and hence the electrical potentials are greater.^[18] But, again the difference in solvation free energy of the three solvation shells shows the same trend: The structure with only 2G is the most stable, followed by the structure with both 2G and THF, and lastly the structure with only THF. Again, this strongly indicates that 2G containing solvation shells are far more likely to co-intercalate and hence would do so at higher potentials vs. Na^+/Na which would open up the graphitic structure for less stable solvation shells to enter.

3. Conclusions

The present study shows for the first time that the solvents THF and DOL can be electrochemically intercalated along with sodium ions at room temperature into graphite. GICs with THF have been prepared earlier by chemical methods but required elevated temperatures. Here instead, following the pore formation model of solvent co-intercalation previously proposed by us, the formation is enabled by the addition of small amounts of 2G molecules to the electrolyte solution and the formation in an electrochemical cell is reversible over several hundreds of cycles (charge/discharge cycles). In other words, the incorporation of additive levels of 2G, or simply low amounts of pre-sodiation in 2G-based electrolytes, enables the reversible co-intercalation of THF and DOL to form compounds with comparable capacity to previously studied t-GICs. *Operando* XRD and ss-NMR were used to study the structure evolution during charging/discharging.

The results suggest the concept of using 2G as a promoter or "gate opener" for the synthesis of GICs. As 2G enables an opening of the graphite structure, other solvents can co-intercalate as well that were previously thought to be unable to do so. The special role of 2G was supported by theoretical calculations which suggest that the interaction between Na^+ and 2G is stronger compared to the other solvents. Changes in the voltage profile further show that the formed compounds are quaternary graphite intercalation compounds (q-GICs), consisting of a cation, graphite and two different types of solvents. These compounds resemble a highly organized two-dimensional structure with properties that are not fully understood.

As an important note, it is reasonable to assume that many of such compounds, even higher-order GICs, exist that may be synthesized using 2G as a promoter. The approach could be also used to design new intercalation electrodes for rechargeable batteries. This is motivated not only by the fact that the redox potential of the graphite electrode can be altered by the type of solvent that is co-intercalated but also because the type of solvent has a strong impact on the lattice expansion/shrinkage ("breathing"), which should be minimized.

Acknowledgements

This project received funding from the European Research Council (ERC) under the European Union's Horizon 2020 research and innovation programme (grant agreement No. [864698], SEED) and from the EIG Concert Japan program (LIBRA, BMBF 01DR18003). Moreover, the authors gratefully acknowledge the computing time granted by the Resource Allocation Board and provided on the supercomputer Lise and Emmy at NHR@ZIB and NHR@Göttingen as part of the NHR infrastructure. The calculations for this research were conducted with computing resources under the project bec00243. Open Access funding enabled and organized by Projekt DEAL.

Conflict of Interests

The authors declare no conflict of interest.

Data Availability Statement

The data that support the findings of this study are available from the corresponding author upon reasonable request.

Keywords: Graphite · Sodium-ion batteries · Co-intercalation · q-GICs · Electrochemistry

- [1] B. Dunn, H. Kamath, J.-M. Tarascon, *Science* **2011**, *334*, 928–935.
- [2] G. G. Eshetu, H. Zhang, X. Judez, H. Adeniusi, M. Armand, S. Passerini, E. Figgemeier, *Nat. Commun.* **2021**, *12*, 5459.
- [3] S. Vadim, A. Nicholas, S. Vijayendra, M. Linqin, M. Lin, *Energy Materials* **2023**, *3*, 300038.
- [4] N. Yabuuchi, K. Kubota, M. Dahbi, S. Komaba, *Chem. Rev.* **2014**, *114*, 11636–11682.
- [5] P. K. Nayak, L. Yang, W. Brehm, P. Adelhelm, *Angew. Chem. Int. Ed.* **2018**, *57*, 102–120.
- [6] H. Kim, H. Kim, Z. Ding, M. H. Lee, K. Lim, G. Yoon, K. Kang, *Adv. Energy Mater.* **2016**, *6*, 1600943.
- [7] O. Lenchuk, P. Adelhelm, D. Mollenhauer, *Phys. Chem. Chem. Phys.* **2019**, *21*, 19378–19390.
- [8] B. Jache, P. Adelhelm, *Angew. Chem. Int. Ed.* **2014**, *53*, 10169–10173.
- [9] I. Escher, Y. Kravets, G. A. Ferrero, M. Goktas, P. Adelhelm, *Energy Technol.* **2021**, *9*, 2000880.
- [10] M. Goktas, B. Akduman, P. Huang, A. Balducci, P. Adelhelm, *J. Phys. Chem. C* **2018**, *122*, 26816–26824.
- [11] M. Goktas, C. Bolli, E. J. Berg, P. Novák, K. Pollok, F. Langenhorst, M. v. Roeder, O. Lenchuk, D. Mollenhauer, P. Adelhelm, *Adv. Energy Mater.* **2018**, *8*, 1702724.
- [12] S. A. Solin, in *Intercalation in Layered Materials* (Ed.: M. S. Dresselhaus), Springer US, Boston, MA, 1986, pp. 291–300.
- [13] J. O. Besenhard, *Carbon* **1976**, *14*, 111–115.
- [14] J. O. Besenhard, H. P. Fritz, *Angew. Chem. Int. Ed. Engl.* **1983**, *22*, 950–975.
- [15] B. Jache, J. O. Binder, T. Abe, P. Adelhelm, *Phys. Chem. Chem. Phys.* **2016**, *18*, 14299–14316.
- [16] H. Kim, J. Hong, Y.-U. Park, J. Kim, I. Hwang, K. Kang, *Adv. Funct. Mater.* **2015**, *25*, 534–541.
- [17] G. Yoon, H. Kim, I. Park, K. Kang, *Adv. Energy Mater.* **2017**, *7*, 1601519.
- [18] G. Ávall, G. A. Ferrero, K. A. Janßen, M. Exner, Y. Son, P. Adelhelm, *Adv. Energy Mater.* **2023**, *13*, 2301944.
- [19] Q. Liu, F. Wu, D. Mu, B. Wu, *Phys. Chem. Chem. Phys.* **2020**, *22*, 2164–2175.
- [20] H. Au, N. Rubio, D. J. Buckley, C. Mattevi, M. S. P. Shaffer, *Chem. - Eur. J.* **2020**, *26*, 6545–6553.
- [21] A. La Monaca, F. De Giorgio, F. Soavi, G. Tarquini, M. Di Carli, P. Paolo Prosini, C. Arbizzani, *ChemElectroChem* **2018**, *5*, 1272–1278.
- [22] M. Orbay, D. Leistenschneider, C. Leibing, A. Balducci, *ChemElectroChem* **2023**, *10*, e202300171.
- [23] S. Xiong, K. Xie, Y. Diao, X. Hong, *J. Power Sources* **2014**, *246*, 840–845.
- [24] H. Zhang, Z. Li, W. Xu, Y. Chen, X. Ji, M. M. Lerner, *Nanotechnology* **2018**, *29*, 325402.
- [25] H.-J. Liang, Z.-Y. Gu, X.-X. Zhao, J.-Z. Guo, J.-L. Yang, W.-H. Li, B. Li, Z.-M. Liu, W.-L. Li, X.-L. Wu, *Angew. Chem. Int. Ed.* **2021**, *60*, 26837–26846.
- [26] D. Saurel, A. Pendashteh, M. Jáuregui, M. Reynaud, M. Fehse, M. Galceran, M. Casas-Cabanas, *Chemistry-Methods* **2021**, *1*, 249–260.
- [27] R. Hoffman, *J. Magn. Reson.* **2022**, *340*, 107231.
- [28] M. J. Frisch, G. W. Trucks, H. B. Schlegel, G. E. Scuseria, M. A. Robb, J. R. Cheeseman, G. Scalmani, V. Barone, G. A. Petersson, H. Nakatsuji, X. Li, M. Caricato, A. V. Marenich, J. Bloino, B. G. Janesko, R. Gomperts, B. Mennucci, H. P. Hratchian, J. V. Ortiz, A. F. Izmaylov, J. L. Sonnenberg, Williams, F. Ding, F. Lipparini, F. Egidi, J. Goings, B. Peng, A. Petrone, T. Henderson, D. Ranasinghe, V. G. Zakrzewski, J. Gao, N. Rega, G. Zheng, W. Liang, M. Hada, M. Ehara, K. Toyota, R. Fukuda, J. Hasegawa, M. Ishida, T. Nakajima, Y. Honda, O. Kitao, H. Nakai, T. Vreven, K. Throssell, J. A. Montgomery Jr., J. E. Peralta, F. Ogliaro, M. J. Bearpark, J. J. Heyd, E. N. Brothers, K. N. Kudin, V. N. Staroverov, T. A. Keith, R. Kobayashi, J. Normand, K. Ragahavachari, A. P. Rendell, J. C. Burant, S. S. Iyengar, J. Tomasi, M. Cossi, J. M. Millam, M. Klene, C. Adamo, R. Cammi, J. W. Ochterski, R. L. Martin, K. Morokuma, O. Farkas, J. B. Foresman, D. J. Fox, Wallingford, CT, 2016.
- [29] A. D. Becke, *Phys. Rev. A* **1988**, *38*, 3098–3100.
- [30] A. D. Becke, *J. Chem. Phys.* **1993**, *98*, 5648–5652.
- [31] C. Lee, W. Yang, R. G. Parr, *Phys. Rev. B* **1988**, *37*, 785–789.
- [32] S. Grimme, J. Antony, S. Ehrlich, H. Krieg, *J. Chem. Phys.* **2010**, *132*.
- [33] A. V. Marenich, C. J. Cramer, D. G. Truhlar, *J. Phys. Chem. B* **2009**, *113*, 6378–6396.
- [34] G. Kresse, J. Furthmüller, *Phys. Rev. B* **1996**, *54*, 11169–11186.
- [35] G. Kresse, J. Furthmüller, *Comput. Mater. Sci.* **1996**, *6*, 15–50.
- [36] G. Kresse, J. Furthmüller, J. Hafner, *Phys. Rev. B* **1994**, *50*, 13181–13185.
- [37] G. Kresse, J. Hafner, *Phys. Rev. B* **1993**, *47*, 558–561.
- [38] G. Kresse, D. Joubert, *Phys. Rev. B* **1999**, *59*, 1758–1775.
- [39] J. P. Perdew, K. Burke, M. Ernzerhof, *Phys. Rev. Lett.* **1996**, *77*, 3865–3868.
- [40] R. Car, M. Parrinello, *Phys. Rev. Lett.* **1985**, *55*, 2471–2474.
- [41] G. Ávall, P. Johansson, *J. Chem. Phys.* **2020**, *152*.
- [42] I. Escher, A. I. Freytag, J. M. López del Amo, P. Adelhelm, *Batteries & Supercaps* **2023**, *6*, e202200421.

- [43] H. Kim, J. Hong, G. Yoon, H. Kim, K.-Y. Park, M.-S. Park, W.-S. Yoon, K. Kang, *Energy Environ. Sci.* **2015**, *8*, 2963–2969.
- [44] G. Alvarez Ferrero, G. Åvall, K. A. Mazzio, Y. Son, K. Janßen, S. Risse, P. Adelhelm, *Adv. Energy Mater.* **2022**, *12*, 2202377.
- [45] M. Wahid, D. Puthusseri, Y. Gawli, N. Sharma, S. Ogale, *ChemSusChem* **2018**, *11*, 506–526.
- [46] N. Karimi, A. Varzi, S. Passerini, *Electrochim. Acta* **2019**, *304*, 474–486.
- [47] I. Escher, M. Hahn, G. Alvarez Ferrero, P. Adelhelm, *Energy Technol.* **2022**, *10*, 2101120.
- [48] B. Rieger, S. Schlueter, S. V. Erhard, J. Schmalz, G. Reinhart, A. Jossen, *J. Energy Storage* **2016**, *6*, 213–221.
- [49] L. Lutz, D. Alves Dalla Corte, M. Tang, E. Salager, M. Deschamps, A. Grimaud, L. Johnson, P. G. Bruce, J.-M. Tarascon, *Chem. Mater.* **2017**, *29*, 6066–6075.
- [50] D. M. C. Ould, S. Menkin, C. A. O'Keefe, F. Coowar, J. Barker, C. P. Grey, D. S. Wright, *Angew. Chem. Int. Ed.* **2021**, *60*, 24882–24887.
- [51] N. Leifer, M. F. Greenstein, A. Mor, D. Aurbach, G. Goobes, *J. Phys. Chem. C* **2018**, *122*, 21172–21184.
- [52] K. Gotoh, H. Maruyama, T. Miyatou, M. Mizuno, K. Urita, H. Ishida, *J. Phys. Chem. C* **2016**, *120*, 28152–28156.
- [53] G. Åvall, J. Mindemark, D. Brandell, P. Johansson, *Adv. Energy Mater.* **2018**, *8*, 1703036.
- [54] E. M. Cabaleiro-Lago, M. A. Ríos, *Chem. Phys.* **1998**, *236*, 235–242.
- [55] A. V. Cresce, S. M. Russell, O. Borodin, J. A. Allen, M. A. Schroeder, M. Dai, J. Peng, M. P. Gobet, S. G. Greenbaum, R. E. Rogers, K. Xu, *Phys. Chem. Chem. Phys.* **2017**, *19*, 574–586.
- [56] E. Flores, G. Åvall, S. Jeschke, P. Johansson, *Electrochim. Acta* **2017**, *233*, 134–141.
- [57] M. He, K. C. Lau, X. Ren, N. Xiao, W. D. McCulloch, L. A. Curtiss, Y. Wu, *Angew. Chem. Int. Ed.* **2016**, *55*, 15310–15314.
- [58] G. Kamath, R. W. Cutler, S. A. Deshmukh, M. Shakourian-Fard, R. Parrish, J. Huether, D. P. Butt, H. Xiong, S. K. R. S. Sankaranarayanan, *J. Phys. Chem. C* **2014**, *118*, 13406–13416.
- [59] D. Monti, E. Jónsson, A. Boschin, M. R. Palacín, A. Ponrouch, P. Johansson, *Phys. Chem. Chem. Phys.* **2020**, *22*, 22768–22777.
- [60] M. Okoshi, C.-P. Chou, H. Nakai, *J. Phys. Chem. B* **2018**, *122*, 2600–2609.
- [61] D. Spångberg, K. Hermansson, *Chem. Phys.* **2004**, *300*, 165–176.
- [62] L. Troxler, G. Wipff, *J. Am. Chem. Soc.* **1994**, *116*, 1468–1480.

Manuscript received: October 30, 2023

Revised manuscript received: January 18, 2024

Accepted manuscript online: January 26, 2024

Version of record online: February 13, 2024
